Adaptive control of unknown unstable steady states of dynamical systems

K. Pyragas,[1,2,*] V. Pyragas,[1] I. Z. Kiss,[3] and J. L. Hudson[3]
[1]*Semiconductor Physics Institute, LT-2600 Vilnius, Lithuania*
[2]*Vilnius Pedagogical University, LT-2004, Vilnius, Lithuania*
[3]*Department of Chemical Engineering, Thornton Hall, University of Virginia, Charlottesville, Virginia 22903-2442, USA*
(Received 19 February 2004; published 30 August 2004)

A simple adaptive controller based on a low-pass filter to stabilize unstable steady states of dynamical systems is considered. The controller is reference-free; it does not require knowledge of the location of the fixed point in the phase space. A topological limitation similar to that of the delayed feedback controller is discussed. We show that the saddle-type steady states cannot be stabilized by using the conventional low-pass filter. The limitation can be overcome by using an unstable low-pass filter. The use of the controller is demonstrated for several physical models, including the pendulum driven by a constant torque, the Lorenz system, and an electrochemical oscillator. Linear and nonlinear analyses of the models are performed and the problem of the basins of attraction of the stabilized steady states is discussed. The robustness of the controller is demonstrated in experiments and numerical simulations with an electrochemical oscillator, the dissolution of nickel in sulfuric acid; a comparison of the effect of using direct and indirect variables in the control is made. With the use of the controller, all unstable phase-space objects are successfully reconstructed experimentally.

DOI: 10.1103/PhysRevE.70.026215 PACS number(s): 05.45.Gg, 82.40.Bj, 82.45.Qr

I. INTRODUCTION

Control theory is one of the central subjects in engineering science. Despite the fact that engineers and applied mathematicians have been dealing with control problems for a long time and a huge amount of knowledge has been gathered [1–4], some new ideas were introduced by physicists a decade ago [5] and have boosted an enormous amount of work on control problems [6–9]. These new concepts are based on the observation that chaotic dynamical systems contain a huge number of unstable periodic orbits. These orbits represent genuine motions of the system and can be stabilized by applying tiny control forces. Hence chaotic dynamics opens the possibility to use flexible control techniques and stabilize quite distinct types of motion in a single system with small control power. A convenient chaos control technique successfully implemented in various experiments is based on delayed feedback perturbation [10]. However, Nakajima [11] proved there is a topological limitation with this technique, namely that it cannot stabilize torsion-free periodic orbits, which are characterized by an odd number of real positive Floquet exponents. It has been recently shown that an additional unstable degree of freedom introduced into a feedback loop can overcome this limitation [12].

Although the field of controlling chaos deals mainly with the stabilization of unstable periodic orbits, the problem of controlling the system dynamics on unstable fixed points (nonoscillatory solutions) could be more important for various technical applications. Controlling the system dynamics on unstable steady fixed points is of practical importance in experimental situations where chaotic or periodic oscillations cause degradation in performance. Usual methods of classical control theory are based on proportional feedback perturbations [4]. They use reference signals that require knowledge of the location of the unstable fixed point in phase space. However, for many complex systems the location of the fixed point, as well as exact model equations, are not accessible. In this case, adaptive, reference-free control techniques, capable of automatically locating the unknown steady state, are preferable.

A straightforward idea to attain an adaptive stabilization of the unknown steady state may be based on derivative control [13,14]. In this approach, the control perturbation is derived from the derivative of an observable. Such a perturbation does not influence the steady-state solutions of the original system, since it vanishes whenever the system approaches the steady state. In practice this method is sensitive to high-frequency fluctuations because it requires a differentiation of a signal. To avoid this shortcoming the derivative may be replaced by a finite difference. Such an idea leads to a time-delay feedback control method. In Ref. [10] it is shown that the time-delay feedback method is indeed capable of stabilizing not only unstable periodic orbits, but unstable steady states as well. These features of the time-delay feedback control method are discussed in more detail in Refs. [15,16]. The theory of the method is rather complicated, since the time-delay feedback involves an infinite number of additional degrees of freedom.

Nevertheless, the problem of adaptive stabilization of fixed points is simpler than the problem of stabilizing unstable periodic orbits and can be successfully solved without the use of time-delay signals. Any adaptive controller, of course, should have inherent degrees of freedom. However, for the fixed points an adaptive controller can be designed on the basis of a finite-dimensional dynamical system. The simplest example of such a controller may utilize a conventional low-pass filter that has only one inherent degree of freedom. The filtered output signal of the system estimates the location of the fixed point, so that the difference between the actual and filtered output signals can be used as a feedback pertur-

*Electronic address: pyragas@pfi.lt; http://pyragas.pfi.lt

 ©2004 The American Physical Society

bation. Such a simple dynamic controller has been successfully implemented in different experiments, including a Mackey-Glass system [16], an electronic chaos oscillator [17], and lasers [18,19]. In Ref. [20], a controller based on a cascade of high-pass filters has been utilized. However, in a short Letter [21] we have recently demonstrated that these controllers have a topological limitation, similar to that of a time-delay feedback controller. They cannot stabilize the steady states with an odd number of real positive eigenvalues. To overcome the limitation, we proposed to implement an unstable degree of freedom in the feedback loop. In this paper, we extend these ideas.

The rest of the paper is organized as follows. In Sec. II, we describe an adaptive controller based on a simple low-pass filter and demonstrate its performance for two simple mathematical models. We show that an unstable focus can be stabilized by a stable controller, while a saddle requires the use of an unstable controller. The efficiency of the controller to stabilize unknown steady states in real physical systems is demonstrated in Sec. III. We consider two systems, namely a pendulum driven with a constant torque and the Lorenz system that describes a chaotic convection in a vertical loop. Section IV is devoted to the problem of controlling an electrodissolution process, the dissolution of nickel in sulfuric acid. We design two adaptive controllers and demonstrate their capability to stabilize unstable foci and saddle steady states in the oscillating regime. We analyze how the restriction of the feedback perturbation influences the size of attraction basins of the stabilized steady states. Experiments are carried out on the stabilization of both saddle- and focus-type unstable states. Lastly, we finish the paper with conclusions presented in Sec. V.

II. ADAPTIVE CONTROLLER

Consider an autonomous dynamical system described by ordinary differential equations

$$\dot{\boldsymbol{x}} = \boldsymbol{f}(\mathbf{x}, p), \tag{1}$$

where the vector $\boldsymbol{x} \in R^m$ defines the dynamical variables and p is a scalar parameter available for an external adjustment. We imagine that a scalar variable

$$y(t) = g(\boldsymbol{x}(t)) \tag{2}$$

that is a function of dynamical variables $\boldsymbol{x}(t)$ can be measured as a system output. Let us suppose that at $p=p_0$ the system has an unstable fixed point $\boldsymbol{x}^*$ that satisfies $\boldsymbol{f}(\boldsymbol{x}^*, p_0) = 0$. If the steady state value $y^* = g(\boldsymbol{x}^*)$ of the observable corresponding to the fixed point were known, we could try to stabilize it by using a standard proportional feedback control, i.e., adjusting the control parameter by the law $p = p_0 - k(y - y^*)$. However, we suppose that the reference value y^* is unknown. Our aim is to construct a reference-free feedback perturbation that automatically locates and stabilizes the fixed point. Such a perturbation should vanish when the system settles on the fixed point. The simplest controller satisfying this requirement can be constructed on a basis of one-dimensional dynamical system

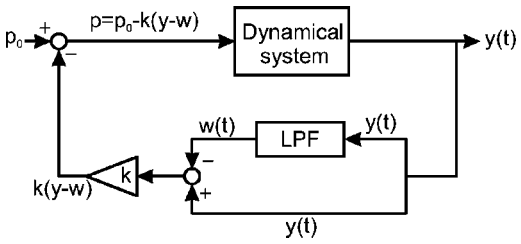

FIG. 1. Block diagram of adaptive control of an unknown steady state of the dynamical system. LPF denotes low-pass filter.

$$\dot{w} = \omega^c (y - w) \tag{3}$$

that represents a simple low-pass filter (LPF). Here w is a dynamical variable of the controller and ω^c represents the cutoff frequency of the filter. The output of the filter gives an averaged input variable $y(t)$. If $y(t)$ oscillates about the steady-state value y^* one can expect that the output variable $w(t)$ converges to this value. Thus the reference value y^* in the proportional feedback control can be replaced with the output variable of the filter. Then the control parameter can be adjusted in the following way:

$$p = p_0 - k(y - w), \tag{4}$$

where k is the control gain. The block diagram of this control technique is shown in Fig. 1. It is similar to the delayed feedback control technique [10], but instead of the delay line we use here a LPF. Note that the whole feedback loop represents a high-pass filter, since the control signal $k(y-w)$ is obtained from the difference of the actual output signal and that filtered by the LPF. The control signal is proportional to the derivative of the controller variable, $k(y-w) = (k/\omega^c)\dot{w}$. For $\omega^c \to \infty$, from Eq. (3) it follows that $w(t) \to y(t)$. Thus for large ω^c the control signal becomes proportional to the derivative of the output $\dot{y}$, and our controller operates as a simple derivative controller. However, using a simple model we shall demonstrate that the best performance of the controller is attained for small values of the cutoff frequency ω^c (smaller values of ω^c can stabilize more unstable steady states). Thus generally this controller cannot be considered as an approximation to a simple derivative approach.

The closed-loop system is described by Eqs. (1)–(4). The feedback perturbation does not influence the location of the original fixed point $\boldsymbol{x}^*$ since the steady-state value of the controller variable w^* coincides with the steady-state value of the observable y^*. In the extended phase space of variables $(\boldsymbol{x}, w)$, the fixed point of the closed-loop system has coordinates $(\boldsymbol{x}^*, y^*)$ so that its projection on the phase space of the free system remains unchanged. However, the perturbation may change the stability of the fixed point.

Small deviations $\delta\boldsymbol{x} = \boldsymbol{x} - \boldsymbol{x}^*$ and $\delta w = w - w^*$ from the fixed point are described by variational equations

$$\delta\dot{\boldsymbol{x}} = J\delta\boldsymbol{x} - kP(G\delta\boldsymbol{x} - \delta w), \tag{5a}$$

$$\delta\dot{w} = \omega^c (G\delta\boldsymbol{x} - \delta w), \tag{5b}$$

where $J = D_{\boldsymbol{x}}\boldsymbol{f}(\boldsymbol{x}^*, p_0)$, $P = D_p\boldsymbol{f}(\boldsymbol{x}^*, p_0)$, and $G = D_{\boldsymbol{x}}\boldsymbol{g}(\boldsymbol{x}^*)$. Here $D_{\boldsymbol{x}}$ denotes the vector derivative with respect to dynamical

variables $\boldsymbol{x}$, and D_p is a scalar derivative with respect to control parameter p. The closed-loop system is linearly stable if all the eigenvalues of the system (5) are in the left half-plane. In a previous paper [21], we provide a theorem concerning an important topological limitation of the above controller. We proved that the controller with the usual LPF cannot stabilize unstable fixed points with an odd number of real positive eigenvalues. To stabilize such fixed points, we need an unstable controller with the negative parameter ω^c. The latter can be built up as an *RC* circuit with a negative resistor. Similar limitation is valid even for a more general case such as the one considered in this paper. It holds when the control parameter p and the controller variable w are the vectors [21].

The above limitation is related to adaptive features of the controller and can be simply explained by bifurcation theory. Suppose that in an extended phase space $(\boldsymbol{x},w)$ the fixed point $(\boldsymbol{x}^*,w^*)$ has an odd total number of real positive eigenvalues. Then if this fixed point is stabilized, one of such eigenvalues must cross into the left half-plane on the real axes. Such a situation corresponds to a tangent bifurcation, which is accompanied by a coalescence of fixed points. However, this contradicts the fact that the feedback perturbation does not change the locations of fixed points. Thus any feedback perturbation that does not change the location of the fixed point can induce stabilization only through a Hopf bifurcation, since this is the only bifurcation that occurs with a single fixed point without any coalescence with other fixed points. At a Hopf bifurcation, a pair of complex-conjugate eigenvalues crosses into the left half-plane. A necessary condition for this bifurcation is that the total number of eigenvalues with positive real parts must be even. Only in this case can complex-conjugate pairs move to the left half-plane. That is why we need an unstable controller $(\omega^c<0)$ when stabilizing a steady state with an odd number of real positive eigenvalues (e.g., a saddle) and we can use a usual LPF with $\omega^c>0$ for the stabilization of a steady state with an even number of real positive eigenvalues (e.g., an unstable focus).

We demonstrate a mechanism of adaptive stabilization of unknown steady states with two simple mathematical examples. The first example describes the control of an unstable focus,

$$\dot{x} = \gamma^s(x - x^*) - (y - y^*), \tag{6a}$$

$$\dot{y} = (x - x^*) + \gamma^s(y - y^*) + p, \tag{6b}$$

$$\dot{w} = \lambda^c(w - y), \quad p = -k(w - y). \tag{6c}$$

Equations (6a) and (6b) represent a normal form of a focus; p is a control parameter. For $p=p_0=0$, the location of the fixed point is (x^*,y^*). We imagine that these coordinates are unknown. Here time is normalized to the period of the focus such that its eigenvalues are $\lambda^s_{1,2}=\gamma^s\pm i$. Parameter $\gamma^s>0$ defines the degree of instability of the focus. Equation (6c) describes an adaptive controller. Instead of the cutoff frequency ω^c, we introduced here the parameter $\lambda^c=-\omega^c<0$ that represents the eigenvalue of the free controller. We suppose that y is an observable and the control parameter p influences only the second equation of the controlled system.

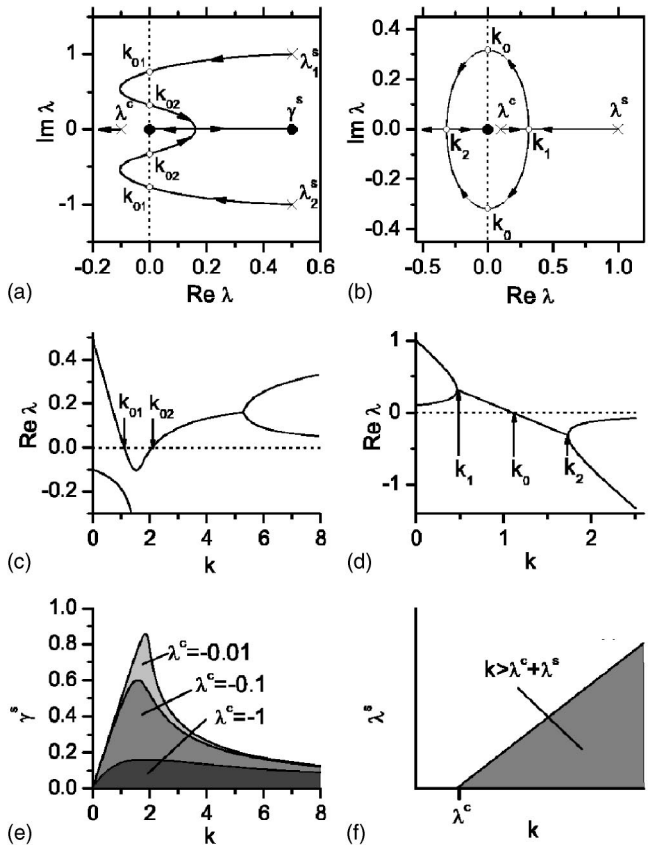

FIG. 2. (a)–(c) Stabilizing an unstable focus with a stable controller in a model of Eqs. (6). (a) Root loci of the characteristic equation (7) as k is varied from 0 to ∞ for $\gamma^s=0.5$ and $\lambda^c=-\omega^c=-0.1$. The crosses and solid dots denote the location of roots at $k=0$ and $k\to\infty$, respectively. (b) Dependence of the real part of eigenvalues on the control gain. (c) Domains of stability of the fixed point in the parameter plane (k,γ^s) for different values of λ^c. (d)–(f) Stabilizing an unstable saddle with an unstable controller in a simple model of Eqs. (8) for $\lambda^s=1$ and $\lambda^c=0.1$. Characteristics are similar to those presented in the left column of the figure.

To analyze the stability of the fixed point (x^*,y^*,y^*) in an extended phase space (x,y,w), it is convenient to shift the origin of the coordinate system to the fixed point by replacing the variables $\delta x=x-x^*$, $\delta y=y^*$, $\delta w=w-y^*$. In these variables, the transfer functions of the system and controller, respectively, are $G(s)=(s-\gamma^s)/[(s-\gamma^s)^2+1]$ and $H(s)=ks/(s-\lambda^c)$. The eigenvalues of the fixed point are determined by poles of the closed-loop system transfer function, i.e., by the equation $1+H(\lambda)G(\lambda)=0$,

$$1 + k\frac{\lambda}{\lambda - \lambda^c}\frac{\lambda - \gamma^s}{(\lambda - \gamma^s)^2 + 1} = 0. \tag{7}$$

A mechanism of stabilization is evident from a root loci diagram presented in Fig. 2(a). The poles and zeros of the product $H(\lambda)G(\lambda)$ define the location of the eigenvalues for $k=0$ and $k\to\infty$, respectively. For $k=0$, there are two complex-conjugate eigenvalues $\lambda=\lambda^s_{1,2}=\gamma\pm i$ in the right half-plane,

corresponding to the free system, and one real eigenvalue $\lambda=\lambda^c=-\omega^c$ in the left half-plane, corresponding to the free controller. As k is increased, the eigenvalue of the controller moves to the left. The complex-conjugate pair of the system roots initially moves to the left as well, and for $k=k_{01}$ these roots cross into the left half-plane (Hopf bifurcation), then return, and for $k=k_{02}$ cross into the right half-plane again (another Hopf bifurcation). Afterwards, they collide on the real axis and one of them moves to the origin of the complex λ plane, and another to the position $\lambda=\gamma^s$. The dependence of the real parts of eigenvalues on the control gain k is shown in Fig. 2(b). In the interval $k_{01}<k<k_{02}$, the real parts of all eigenvalues are negative and the steady state of the closed-loop system is stable. Figure 2(c) shows the domains of stability of the closed-loop system in the parameter plane (k,γ^s) for different values of the cutoff frequency $\omega^c=-\lambda^c$ of the low-pass filter. The properties of the controller are improved by decreasing the cutoff frequency ω^c. Smaller values of ω^c can stabilize more unstable foci. However, the controller cannot stabilize a strongly unstable focus where $\gamma^s>1$. This limitation is due to the configuration of the coupling of the feedback force. The feedback perturbs only one variable [Eq. (6b)] of the focus. For this coupling configuration, the same limitation is valid in the case of proportional feedback control. Note that this limitation is not inherent to the control algorithm. For a fixed coupling configuration, one can design a higher-order adaptive controller that can stabilize any focus with arbitrary large parameter γ^s.

The second example illustrates the use of an unstable controller in the case of an even number of real positive eigenvalues. The simplest representative of such a type is a one-dimensional dynamical system $\dot{y}=\lambda^s(y-y^*)$ that has an unstable fixed point y^* with only one real positive eigenvalue $\lambda^s>0$. The system controlled by the adaptive controller is described by the equations

$$\dot{y}=\lambda^s(y-y^*)+p, \tag{8a}$$

$$\dot{w}=\lambda^c(w-y), \quad p=-k(w-y). \tag{8b}$$

Now the transfer function of the system is $G(s)=1/(s-\lambda^s)$ and the eigenvalues of the closed-loop system satisfy an equality

$$1+k\frac{\lambda}{\lambda-\lambda^c}\frac{1}{(\lambda-\lambda^s)}=0 \tag{9}$$

that is equivalent to the quadratic equation $\lambda^2-(\lambda^s+\lambda^c-k)\lambda+\lambda^s\lambda^c=0$. The stability conditions of this characteristic equation are $k>\lambda^s+\lambda^c$, $\lambda^s\lambda^c>0$. We see that the stabilization is not possible with a conventional low-pass filter since for any $\lambda^s>0$, $\lambda^c<0$, we have $\lambda^s\lambda^c<0$ and the second stability criterion is not met. However, the stabilization can be attained via an unstable controller with a positive parameter λ^c (or negative cutoff frequency ω^c). The right column of Fig. 2 shows similar characteristics to those of the previous model. The root loci diagram [Fig. 2(d)] demonstrates a mechanism of stabilization. For $k=0$, the eigenvalues are λ^s and λ^c, which correspond to the free system and free controller, respectively. With the increase of k, they approach each other on the real axes, then collide at $k=k_1\equiv\lambda^s+\lambda^c-2\sqrt{\lambda^s\lambda^c}$ and pass to the complex plane. At $k=k_0\equiv\lambda^s+\lambda^c$, they cross symmetrically into the left half-plane (Hopf bifurcation). At $k=k_2\equiv\lambda^s+\lambda^c+2\sqrt{\lambda^s\lambda^c}$, we have again a collision on the real axes and then one of the roots moves towards $-\infty$ and another approaches the origin. For $k>k_0$, the closed-loop system is stable. An optimal value of the control gain is k_2 since it provides the fastest convergence to the fixed point.

Note that both models considered here are linear. Thus the defined stability criteria are global, i.e., they are valid for any initial conditions. For nonlinear systems, the linear stability guarantees the stabilization of the steady state only for the initial conditions that are close to the fixed point. In a real physical system, the domain of attraction of the linearly stabilized fixed point depends on specific nonlinear properties of the system. In Sec. IV we consider this problem in more detail.

III. APPLICATION TO PHYSICAL MODELS

In this section we illustrate the efficiency of the adaptive controller for two physical models. First we use an unstable controller to stabilize a saddle steady state of a pendulum driven by a constant torque. Then we demonstrate an adaptive stabilization of all unstable steady states in a chaotic flow described by the Lorenz system.

A. Control of a pendulum driven by a constant torque

Consider a simple mechanical example of a nonlinear oscillator: a pendulum driven by a constant torque. The equation of motion in dimensionless form reads

$$\ddot{\Theta}+\beta\dot{\Theta}+\sin\Theta=\gamma. \tag{10}$$

Here Θ denotes the angle between the pendulum and the downward vertical (see the inset in Fig. 3). $\beta=b/mL^{3/2}g^{1/2}$ and $\gamma=\Gamma/mgL$ are the dimensionless parameters, where m is the mass and L is the length of the pendulum, b is a viscous damping constant, g is the acceleration due to gravity, and Γ is an applied constant torque. The time is normalized to a period $T=(L/g)^{1/2}$ of small oscillations of the free pendulum.

For small torque $\gamma<1$, the pendulum has two equilibrium steady states whose coordinates in $(\Theta,\dot{\Theta})$ phase plane are $(\Theta_s,0)$ and $(\Theta_u,0)$, where $\Theta_s=\arcsin\gamma$ and $\Theta_u=\pi-\arcsin\gamma$. In these steady states the gravity balances the applied torque. The first is a stable node or spiral and the second is a saddle point. Our goal is to stabilize the saddle point $(\Theta_u,0)$ by using an unstable adaptive controller based on the *RC* circuit with a negative resistance.

We suppose that an observable is the angle Θ, and that we can control the system by applying a feedback perturbation to the torque γ. Then our controlled system is

$$\dot{\Theta}=\Omega, \tag{11a}$$

$$\dot{\Omega}=-\beta\Omega-\sin\Theta+\gamma+k(w-\Theta), \tag{11b}$$

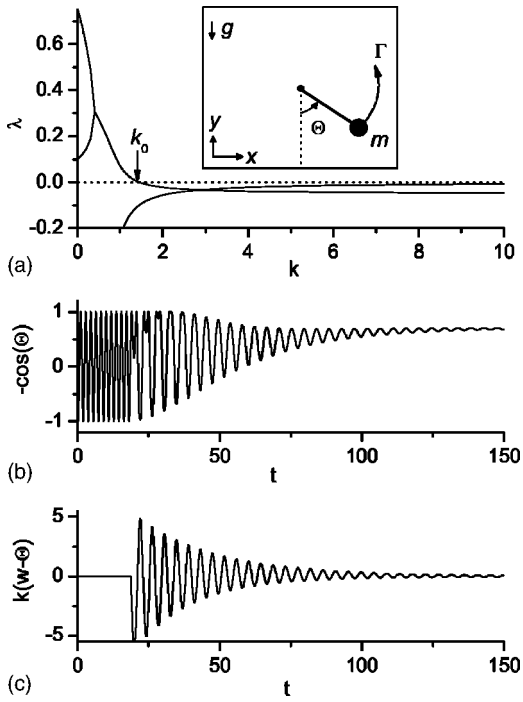

FIG. 3. Stabilizing a saddle steady state of the pendulum driven by a constant torque. (a) Eigenvalues of the controlled pendulum as functions of the control gain k. (b) The dynamics of the y projection of the pendulum. (c) The dynamics of the perturbation. The parameters are $\beta=0.2$, $\gamma=0.7$, $\lambda^c=0.1$. In (b) and (c), the feedback perturbation is switched on at the moment $t=t_c=20$ and the value of control gain is $k=2.6$.

$$\dot{w} = \lambda^c(w - \Theta). \tag{11c}$$

The controller can stabilize the saddle steady state of the pendulum if the fixed point $(\Theta_u, 0, \Theta_u)$ of the controlled system (11) in the extended phase space of variables (Θ, Ω, w) is stable. Linearization of the system (11) about this fixed point yields the characteristic equation

$$\lambda^3 + (\beta - \lambda^c)\lambda^2 + (k - \sqrt{1-\gamma^2} - \lambda^c\beta)\lambda + \lambda^c\sqrt{1-\gamma^2} = 0. \tag{12}$$

The fixed point is linearly stable if all the roots of Eq. (12) have negative real parts. Using the well-known Routh-Hurwitz criteria [22], one obtains the following stability conditions:

$$k > k_0 \equiv \beta[\lambda^c + \sqrt{1-\gamma^2}/(\beta - \lambda^c)], \quad 0 < \lambda^c < \beta. \tag{13}$$

As is expected from a general theory, the necessary stability condition is $\lambda^c > 0$, i.e., the saddle steady state can be stabilized only with an unstable controller.

Figure 3(a) shows the real parts of eigenvalues λ as functions of the control gain k. Similar to the above simple example, the real positive eigenvalues of the pendulum and controller collide on the real axis, pass to the complex plane, and at $k=k_0$ cross into the left half-plane. The results of direct numerical integration of the nonlinear system (11) are presented in Figs. 3(b) and 3(c). The initial condition of the controller at the moment of switching on the control $t=t_c=19$ coincides with the current value of the angle, $w(t_c)=\Theta(t_c)$. The parameters are chosen in such a way that the uncontrolled pendulum is in a multistable regime: depending on initial conditions it can settle into either a rotating solution where it whirls over the top, or a stable rest state Θ_s where the gravity balances the applied torque. For the same values of parameters, there is a coexisting unstable rest state Θ_u of a saddle type. Figure 3(b) shows how the rotating pendulum reaches this state, after applying the feedback perturbation. As is seen from Fig. 3(c), the perturbation vanishes as the stabilization of the saddle steady state is attained. Remember that our controller is reference-free, i.e., it does not utilize knowledge of the position of the fixed point. Thus it can be used for a tracking procedure. The controlled system will remain in the stabilized saddle state even under a slow variation of the applied torque.

B. Control of the Lorenz system

Now we consider the control of stability of the steady states in a chaotic system described by the Lorenz equations [23]

$$\dot{x} = \sigma(y - x), \tag{14a}$$

$$\dot{y} = rx - y - xz, \tag{14b}$$

$$\dot{z} = xy - bz. \tag{14c}$$

Originally this model has been derived and analyzed in the context of turbulent convection. Fortunately, there is a simple physical realization of the Lorenz model: convection in a vertical loop (see the inset in Fig. 4) [24,25]. The fluid is heated from below, and for strong enough heating, convection sets in. The motion is first steady, with a constant velocity V. Clearly, due to symmetry, motions in both the clockwise and counterclockwise directions are possible. If the heating from below increases, the steady rotation becomes unstable and chaotic reversions of the flow are observed. In the context of the above experiment, the variables of the Lorenz equations have the following physical meaning: x is proportional to the flow velocity V, y is proportional to the horizontal temperature difference $T_3 - T_1$, and z is proportional to the vertical temperature difference $T_4 - T_2$. σ, b, and r are dimensionless parameters. When analyzing the Lorenz system, the parameters σ and b are usually fixed to the values 10 and 8/3, respectively. The parameter r is proportional to the heating rate at the bottom and is usually taken as a main control parameter.

For $0<r<1$, the Lorenz system has a unique stable steady state (a stable node) at the origin $(x,y,z)=(0,0,0)$. For $r>1$, the origin becomes a saddle. This means that the motionless state of the liquid loses stability. Just at this bifurcation two additional symmetrical stable steady states $\mathbf{(}[b(r-1)]^{1/2}, [b(r-1)]^{1/2}, r-1\mathbf{)}$ and $\mathbf{(}-[b(r-1)]^{1/2}, -[b(r-1)]^{1/2}, r-1\mathbf{)}$ appear. They correspond to the stationary motion of the liquid with constant velocity. For $r > r_h = \sigma(\sigma+b+3)/(\sigma-b-1)$, these fixed points lose their stability and become unstable spirals. Now a chaotic motion of the liquid is

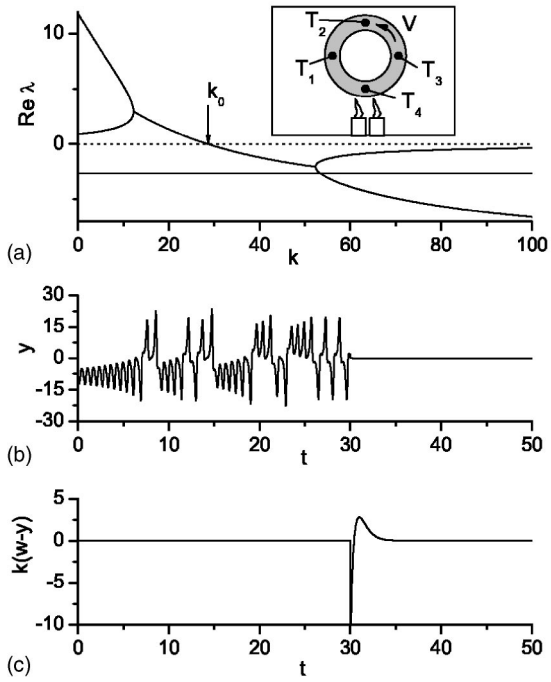

FIG. 4. Stabilizing a saddle steady state (nonconvective state) of the Lorenz system with an unstable controller. (a) Eigenvalues of the controlled Lorenz system as functions of the control gain k. (b) The dynamics of the y variable. (c) The dynamics of the perturbation. The parameters are $\sigma=10$, $b=8/3$, $r=28$, $\lambda^c=1$. In (b) and (c), the feedback perturbation is switched on at the moment $t=t_c=30$. The initial condition of the controller at this moment coincides with the observable y, $w(t_c)=y(t_c)$. The value of control gain is $k=55$.

observed in the system. Our aim is to stabilize all unstable steady states of the system in a chaotic regime for $r>r_h$ using the above adaptive dynamic controller.

We suppose that the observable is y and we can influence the temperature difference T_3-T_1 by additional heating of the loop in the horizontal direction. Then we analyze the controlled Lorenz system described by the following equations:

$$\dot{x} = \sigma(y - x), \tag{15a}$$

$$\dot{y} = rx - y - xz + k(w - y), \tag{15b}$$

$$\dot{z} = xy - bz, \tag{15c}$$

$$\dot{w} = \lambda^c(w - y). \tag{15d}$$

We start with the problem of stabilizing the motionless steady state, i.e., the saddle fixed point at the origin. This fixed point has one positive and two negative real eigenvalues. Thus it can be stabilized only with an unstable controller with the positive parameter λ_c. Indeed, linearizing the system (15) about the origin $(x,y,z,w)=(0,0,0,0)$, we obtain that one eigenvalue is independent of k and is negative $\lambda=-b$, and three remaining eigenvalues satisfy the characteristic equation

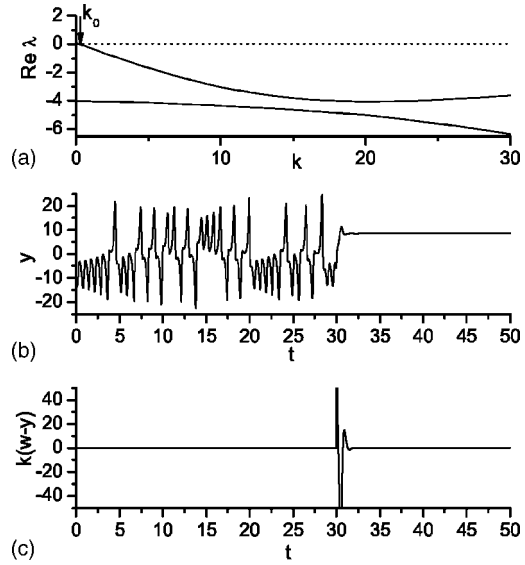

FIG. 5. Stabilizing an unstable spiral (convective state with a constant velocity of the fluid) of the Lorenz system with a stable controller. The values of the parameters are the same as in Fig. 4, except λ^c and k, which that here are equal to -4 and 20, respectively.

$$\lambda^3 + (\sigma + 1 - \lambda^c + k)\lambda^2 + [\sigma(1 - r - \lambda^c + k) - \lambda^c]\lambda + \sigma\lambda^c(r - 1) = 0. \tag{16}$$

The necessary condition of stability of the polynomial (16) is $\sigma\lambda^c(r-1)>0$. The latter can be satisfied only with an unstable controller, $\lambda^c>0$. Using the Routh-Hurwitz criteria [22] one can obtain the threshold of the stability k_0. For $\sigma=10$, $r=28$, and sufficiently small λ^c the stability condition reads

$$k > k_0(\lambda^c) \approx 27 + 1.81\lambda^c. \tag{17}$$

Figure 4(a) shows the three largest real parts of eigenvalues as functions of the control gain k. The horizontal line in this figure corresponds to the eigenvalue $\lambda=-b$ that is independent of k. The results of direct integration of the nonlinear system (15) are shown in Figs. 4(b) and 4(c). Initially the system is in a chaotic regime. When the perturbation is switched on, the system is forced to the rest state. Whenever the stabilization of the rest state is attained, the feedback perturbation vanishes.

Similar results of adaptive stabilization of the unstable spirals $\mathbf{(}\pm[b(r-1)]^{1/2}, \pm[b(r-1)]^{1/2}, r-1\mathbf{)}$ are shown in Fig. 5. These fixed points correspond to the stationary motion of the liquid in clockwise and counterclockwise directions with the constant velocity. They have identical stability conditions and, depending on initial conditions, the system can be stabilized to either of these states. The unstable spirals have one real negative eigenvalue and a complex-conjugate pair of eigenvalues with the positive real part. Thus we use a stable controller for the stabilization. Physically, this stabilization means that chaotic convection of the system is transformed into regular convection with a constant velocity of the liquid.

We emphasize that this state can be maintained by applying only tiny feedback perturbations.

IV. CONTROL OF AN ELECTROCHEMICAL OSCILLATOR

Lastly, we demonstrate the use of an adaptive controller with control in an electrodissolution process, the dissolution of nickel in sulfuric acid. A model for the galvanostatic dissolution (constant current) has been developed by Haim *et al.* [26]. A form of this model, modified for potentiostatic (constant applied potential) operation, describes the steady-state dependence on the potential, bistability, and periodic oscillatory behavior. The dimensionless model reads

$$\dot{e} = (V - e)/R - f_3(e)(1 - \Theta), \tag{18a}$$

$$\Gamma_1 \dot{\Theta} = f_1(e)(1 - \Theta) - f_2(e)\Theta. \tag{18b}$$

Here e is the dimensionless potential of the Ni electrode and Θ is the surface coverage of NiO+NiOH. The functions in the above expressions are

$$f_1(e) = \frac{\exp(0.5e)}{1 + C_h \exp(e)}, \tag{19a}$$

$$f_2(e) = \frac{bC_h \exp(2e)}{C_h C + \exp(e)}, \tag{19b}$$

$$f_3(e) = C_h f_1(e) + a\ \exp(e). \tag{19c}$$

An observable is the current through the Ni electrode,

$$i = (V - e)/R, \tag{20}$$

where R is the series resistance of the cell, and V is the circuit potential—the main experimentally controlled parameter. We shall control the system dynamics by varying this parameter $V = V_0 + \delta V$ with the feedback signal δV derived from the observable $i(t)$. But first we consider the steady-state solutions and dynamical properties of the free system, when $\delta V = 0$, i.e., $V = V_0 = \text{const}$.

A. Analysis of the system without control

For a fixed voltage $V = V_0$, the steady-state solutions (e_0, Θ_0) of the system (18) are determined by equations

$$(V_0 - e_0)/R - f_3(e_0)(1 - \Theta_0) = 0, \tag{21a}$$

$$f_1(e_0)(1 - \Theta_0) - f_2(e_0)\Theta_0 = 0. \tag{21b}$$

These equations are linear with respect to variables V_0 and Θ_0. Thus we can easily obtain explicit expressions

$$\Theta_0 = \Theta_0(e_0) = \frac{f_1(e_0)}{f_1(e_0) + f_2(e_0)}, \tag{22a}$$

$$V_0 = V_0(e_0) = e_0 + R\frac{f_2(e_0) f_3(e_0)}{f_1(e_0) + f_2(e_0)} \tag{22b}$$

that define the steady-state characteristics of the system in a parametric form (e_0 is interpreted as an independent parameter). The steady characteristics e_0 vs V_0 and i vs V_0 are shown in Fig. 6. We see that in a certain interval of the potential V_0 the system has three coexisting fixed points. The linear analysis of these points shows that the lower branch in Fig. 6(a) corresponds to an unstable spiral, the middle branch represents a saddle, and the upper branch is a stable node.

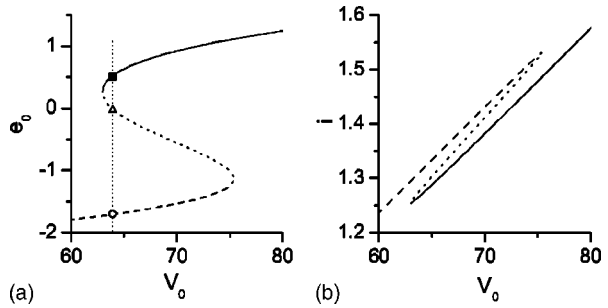

FIG. 6. Steady-state characteristics of the chemical reaction obtained from Eqs. (21). The dashed line represents an unstable spiral, the dotted line corresponds to a saddle, and the solid line is a stable node. The values of the parameters are $R = 50$, $\Gamma_1 = 10^{-2}$, $b = 6 \times 10^{-5}$, $C_h = 1600$, $C = 10^{-3}$, and $a = 0.3$.

Now we discuss the bifurcations that appear in the system when varying the control parameter V_0. The phase portraits of the system for different values of V_0 are shown in Fig. 7. The results are presented in the delayed phase-space coordinates $(i(t), i(t-\tau))$ using the observable $i(t)$. Such a choice of the phase-space variables allows us to compare the numerical results with the experimental ones.

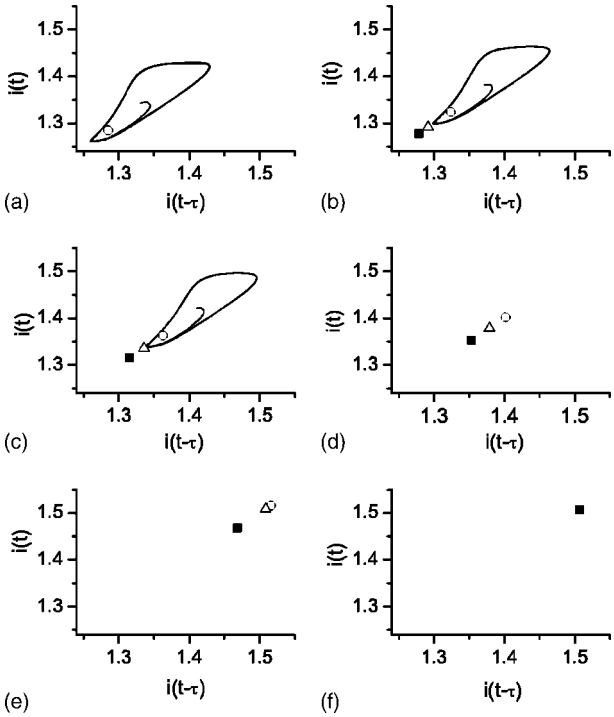

FIG. 7. Phase portraits of the free chemical system presented in delayed coordinates ($\tau = 0.94$) for different values of the voltage V_0: (a) 62.5, (b) 64.5, (c) 66.5, (d) 68.5, (e) 74.5, (f) 76.5. The circles, triangles, and squares denote unstable spirals, saddles, and stable nodes, respectively. The values of the parameters are the same as in Fig. 6.

For small values V_0, an unstable spiral is the only steady state of the system. This spiral is surrounded by a stable limit cycle that corresponds to chemical oscillations [Fig. 7(a)]. The increase of V_0 leads to a saddle-node bifurcation at which two additional fixed points appear [Fig. 7(b)]. Then the saddle collides with the limit cycle [homoclinic bifurcation, Fig. 7(c)], and the limit cycle disappears [Fig. 7(d)]. The further increase of V_0 leads to another saddle-node, bifurcation [Fig. 7(e)], and the only one fixed point, a stable node, remains in the system [Fig. 7(f)].

Next, we fix the value of the voltage $V_0=63.888$ [in Fig. 6(a) this value is marked by a vertical dotted line]. Then the system has two unstable fixed points: a saddle and an unstable spiral, whose coordinates (e_0,Θ_0) are $(0.0,0.0166)$ and $(-1.7074,0.4521)$, respectively. We consider the problem of stabilizing these unstable states by using two different strategies. In the first, the value of the potential e is taken as a control signal. We suppose that this value can be reconstructed from the observable i. In the second, we design the controller that uses directly the observable i.

B. Stabilization using the potential as a control signal

Since the input variable, the voltage V, perturbs only the first differential equation of the system (18), it is natural to construct the perturbation in such a way that it introduces a negative feedback to the potential e. If the value of the circuit resistance R is known, then the value of the potential e can be reconstructed from the observable i and input variable V: $e=V-iR$. However, the exact value R is unknown in an experiment. Then we propose to use the difference $\tilde{e}=V-ir$ as an effective control signal, where r is an adjustable control parameter that need not be exactly equal to the circuit resistance R. We shall see that the stabilization can be attained for $r\neq R$ as well.

Here we restrict ourselves to the problem of stabilizing the saddle steady state that requires use of an unstable controller. We define an unstable controller for an effective potential $\tilde{e}$ by the differential equation

$$\frac{dw}{dt}=\lambda^c(w-\tilde{e})=\lambda^c(w-V+ir), \tag{23}$$

where w is a dynamic variable of the controller and λ^c is a positive constant. Now we feed back the control perturbation $\delta V=k(w-V+ir)$ to the adjustable parameter V,

$$V=V_0+k(w+ir-V). \tag{24}$$

Solving this equation together with Eq. (20), we obtain the expression for the voltage,

$$V=\frac{V_0+k(w-e/R)}{1+k(1-r/R)}, \tag{25}$$

where k is the control gain. Thus the controlled chemical system is defined by differential equations (18) and (23), and algebraic expressions (19), (20), and (25). Note that the introduced controller does not change the steady-state solutions of the free chemical system. Indeed, the stationary state of the controller is determined by the equality $w-V+ir=0$.

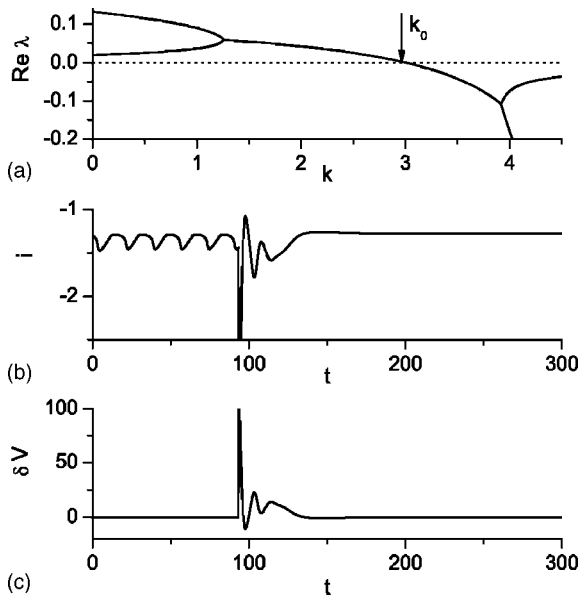

FIG. 8. Stabilizing a saddle steady state of the chemical system using the potential as a control signal. (a) Eigenvalues of the controlled chemical system as functions of the control gain k. (b) and (c) The dynamics of the current and perturbation, respectively. In (b) and (c), the feedback perturbation is switched on at the moment $t=t_c=93$. The parameters of the controller are $\lambda^c=0.02$, $r=60$, and $k=3.9$.

Thus the perturbation added to the voltage is equal to zero, and from Eq. (24) we obtain that $V=V_0$. The steady-state value of the controller variable is $w_0=V_0(1-r/R)+e_0r/R$ and the corresponding fixed point of the controlled chemical system in the whole phase space of variables (e,Θ,w) is (e_0,Θ_0,w_0), where e_0,Θ_0 are the steady-state solutions of the free chemical system. Linearizing Eqs. (18) and (23) about this fixed point, one can obtain the stability conditions. Figure 8(a) shows the eigenvalues of the saddle fixed point $(e_0,\Theta_0,w_0)=(0.0,0.1666,-12.7776)$ taken at the voltage $V_0=63.888$, as functions of the control gain k. For $k>k_0\approx 2.97$, the saddle steady state of the free systems becomes stable due to introduced feedback control. This result of a linear theory is confirmed by direct integration of nonlinear Eqs. (18) and (23). Figures 8(b) and 8(c) show the dynamics of the current and perturbation, respectively, for $k=0.02$. At the moment of switching on the control $t=t_c\approx 93$ the initial condition for the controller is $w(t_c)=\tilde{e}(t_c)$. Note that the parameter r is chosen not equal to R ($r=60$ and $R=50$). Although an effective potential $\tilde{e}$ does not coincide with the real potential e, the stabilization of the fixed point is still possible.

C. Stabilization using the current as a control signal

The controller described in the preceding paragraph is based on reconstruction of the potential e and implementation of a negative feedback to this variable. Now we consider another controller that does not require any reconstructions of dynamic variables and is particularly convenient for experimental implementation. We take the observable $i(t)$ as a

control signal, then transform it by an adaptive dynamic controller and feed back the output to the control parameter $V(t)$. Specifically, we define an adaptive controller by the differential equation

$$\frac{dw}{dt} = \lambda^c(w - i), \tag{26}$$

where w is a dynamic variable of the controller and λ^c is a characteristic parameter. Then we feed back the control perturbation $\delta V = k(i - w)$ to the input voltage V,

$$V = V_0 + \delta V = V_0 + k(i - w), \tag{27}$$

where k is the control gain. Substituting this expression in Eq. (20) and solving it with respect to an unknown current, we obtain $i = (V_0 - e - kw)/(R - k)$. Then from Eq. (27) we get the following expression for the voltage:

$$V = V_0 + k\frac{V_0 - e - wR}{R - k}. \tag{28}$$

We see that voltage perturbation is singular for $k = R$. The controlled chemical system is defined by the differential equations (18) and (26), and algebraic expressions (19), (20), and (28). This controller, as well as that considered before, does not change the steady-state solutions of the free chemical system. Whenever the controller attains the steady state, $dw/dt = 0$, the voltage perturbation $\delta V = k(i - w)$ vanishes. The steady-state value of the controller variable coincides with the steady-state value of the current of the unperturbed system, $w_0 = i_0 = (V_0 - e_0)/R$. Thus the fixed point of the controlled chemical system in the whole phase space of variables (e, Θ, w) is (e_0, Θ_0, i_0). Linearizing Eqs. (18) and (26) about this fixed point, one can obtain the dependence of its eigenvalues on the control gain k. For the unstable spiral $(e_0, \Theta_0, i_0) = (-1.7074, 0.4521, 1.3119)$, taken at the voltage $V_0 = 63.888$, this dependence is shown in Fig. 9(a). For $k > k_0 \approx 46.2$, the initially unstable spiral becomes stable. Figures 9(b) and 9(c) show the results of a nonlinear analysis. The dynamics of the current and perturbation are obtained by direct integration of a nonlinear system of Eqs. (18) and (26). At the moment of switching on the control $t = t_c = 90$, the initial condition for the controller is taken to be equal to the current, $w(t_c) = i(t_c)$. Again, the current of the controlled chemical system asymptotically converges to the unperturbed steady-state value i_0 and the perturbation vanishes.

To stabilize the unstable spiral, we used a stable controller with the negative parameter $\lambda^c = -0.01$. Figure 10 shows similar results of stabilizing the saddle point $(e_0, \Theta_0, i_0) = (0.0, 0.0166, 1.27778)$ taken at the same voltage $V_0 = 63.888$. However, now an unstable controller with the positive parameter $\lambda^c = 0.01$ has been used.

Note that the controller considered in this subsection has only one adjustable parameter λ^c, while the controller based on reconstruction of the potential e has two adjustable parameters, λ^c and r. Thus this controller is more convenient for experimental implementation.

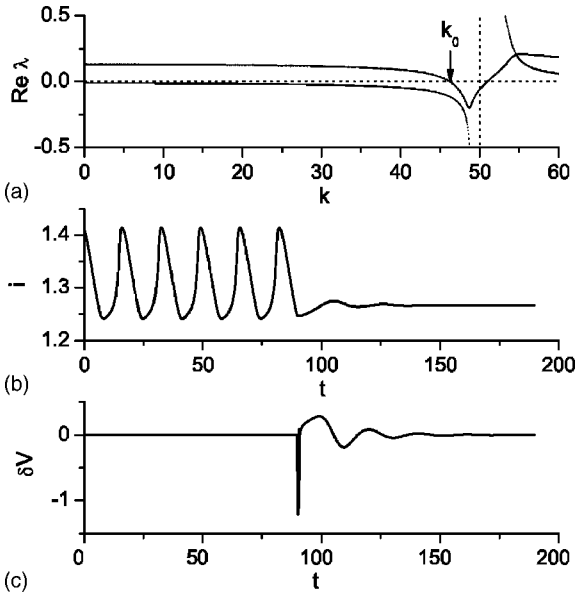

FIG. 9. Stabilizing an unstable spiral of the chemical system using the current as a control signal. (a) Eigenvalues of the controlled chemical system as functions of the control gain k. (b) and (c) The dynamics of the current and perturbation, respectively. In (b) and (c), the feedback perturbation is switched on at the moment $t = t_c = 90$. The parameters of the controller are $\lambda^c = -0.01$ and $k = 49.9$.

D. Restriction of perturbation and basins of attraction

The linear stability of a fixed point of dynamical system guarantees its stabilization only for initial conditions that are close to the fixed point. Important questions arise concerning what is the basin of attraction of a linearly stable fixed point in the phase space of nonlinear system and how to control the size of this basin. These questions are especially signifi-

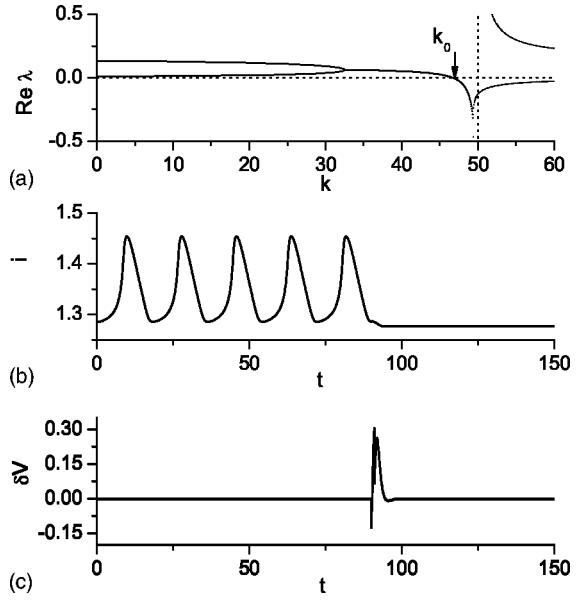

FIG. 10. The same as in Fig. 9 but for the saddle fixed point controlled by an unstable controller with the parameter $\lambda^c = 0.01$.

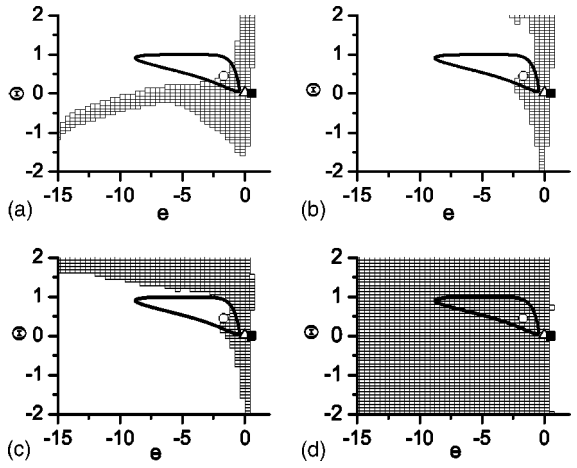

FIG. 11. Basins of attraction of the stabilized saddle steady state of the chemical system (a) without restriction of the perturbation, and for restricted perturbation with different values of $\delta V_{\max}$: (b) 100, (c) 50, and (d) 25. The solid line, as well as in Fig. 7, represents the limit cycle. The circles, triangles, and squares denote the spiral, saddle, and node, respectively.

cant from an experimental point of view. Generally, there is no analytical approach to answer these questions. The basins of attraction can be obtained numerically by direct integration of the underlying differential equations for different values of initial conditions. We performed such an analysis for the chemical system in the case when the current is used as a control signal. The basin of attraction in the (e,Θ) phase plane for the stabilized saddle fixed point is presented in Fig. 11(a). The initial condition for the controller is taken equal to the initial value of the current, $w(0)=i(0)=[V_0-e(0)]/R$. We see that only a small part of the limit cycle resides in the basin of attraction of the saddle point. This means that the control will not always be successful if we try to switch the system behavior from a regime of limit cycle oscillations to a saddle steady state. We succeed in our intention only if we switch on a control at a proper moment when the phase of limit cycle oscillations is in the basin of attraction of the saddle steady state. If the control is switched on at an improper moment, the feedback perturbation increases rapidly and the system runs far away from the saddle point and limit cycle. A natural way to avoid such runaways is to restrict the perturbation.

We analyzed the system behavior under the following algorithm of the restriction. When the absolute value of the perturbation $|\delta V|$ reaches some maximum $\delta V_{\max}$, we zero the perturbation by changing the state of the controller. Let t_m be the moment when the perturbation reaches the maximum of the allowable amplitude, $|\delta V(t_m)|=\delta V_{\max}$. At this moment we change the state of the controller setting the variable w equal to the current, $w(t_m)=i(t_m)$. From Eq. (27) it follows that the perturbation at this moment turns to zero $\delta V(t_m)=0$. Figures 11(b)–11(d) show an evolution of the basin of attraction when varying the parameter $\delta V_{\max}$. For sufficiently small $\delta V_{\max}$, the basin of attraction becomes rather large so that the limit cycle totally resides in the basin of attraction [Fig. 11(d)]. In this case the system behavior can be changed from periodic limit cycle oscillations to a saddle steady state by switching on the control at any moment independently of the phase of oscillations. Thus the constrained perturbations can essentially improve the control of the dynamical system in a real experiment.

In a similar manner, we analyzed the basin of attraction for the spiral fixed point. The analysis shows that this basin is rather large [similar to that presented in Fig. 11(d)] even without restriction of the perturbation. The different sizes of attraction basins for the spiral and saddle fixed points are probably related to different controllers used for the stabilization. For the saddle fixed point, we used the unstable controller, while the spiral is stabilized with the stable one. The unstable controller increases the probability of runaway that can be avoided with a restriction on the perturbation. The stable controller does not introduce any additional instabilities to the system and the restriction of the perturbation is not essential.

E. Experiment

Laboratory experiments have been carried out with nickel dissolution to verify the applicability of the proposed controllers. A standard electrochemical cell consisting of a nickel working electrode (1 mm diam), a $Hg/Hg_2SO_4/K_2SO_4$ reference electrode, and a Pt mesh counterelectrode was used. The current of the electrode is measured with a zero resistance ammeter, and the potential of the electrode is controlled with a Keithley Adwin Pro online controller system connected to the potentiostat. The data acquisition and control frequency was 200 Hz, larger than the inherent frequency of the oscillations (<1 Hz).

The experimental parameters (concentration of sulfuric acid 4.5 M, added external resistance 602 Ω, circuit potential, V_0) have been optimized to show similar dynamics to those of the simulations. At $V_0=1.240$ V, periodic oscillations and a low-current, stable steady state are seen. (At a higher potential, about $V_0=1.270$ V, the oscillations disappear with finite amplitude and infinite period characteristic of a saddle loop bifurcation.) In this parameter region, the model predicts the existence of two additional unstable steady states, namely a high current unstable focus inside the limit cycle and a saddle point between the lower stable and the higher unstable one.

The stabilization of these latter two steady states has been performed by implementing the two above-described control techniques. Figure 12 shows successful stabilization of a saddle steady state by using the potential as a control signal, when the the control algorithm is described by Eqs. (23) and (24). As soon as the control is turned on, the system approaches the saddle point. After turning the control off, the system returns to the original limit cycle. The control is not perfect; the perturbations decay to a nonzero value. Small offset of the perturbations was always observed using the potential as observable. This method also requires a small enough value of restriction $\delta V_{\max}\approx 50$ mV. At large $\delta V_{\max}$ (e.g., 100–200 mV) the offset can also be large, and successful control is difficult to obtain.

Better results have been obtained using the current as an observable, i.e., with the algorithm based on Eqs. (26) and

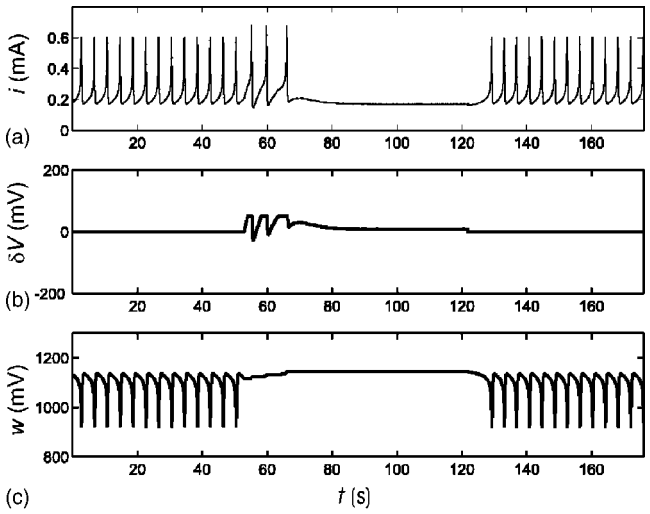

FIG. 12. Control of a saddle point using the potential as a control signal. Control algorithm is described by Eqs. (23) and (24). (a) Dynamics of the current i. (b) Dynamics of the perturbation δV. (c) Dynamics of the controller variable w. $V_0=1.24$ V, $r=602\ \Omega$, $k=200$, $\lambda^c=0.1\ s^{-1}$, $\delta V_{max}=50$ mV.

(27). Figure 13 shows results similar to those presented in Fig. 12, but obtained with the latter control algorithm. The control is achieved without an apparent offset, and is not sensitive to the choice of δV_{max}.

The same control algorithm has been applied to stabilize the unstable focus inside the limit cycle. This has been achieved by changing only the sign of the parameter λ^c, thus converting the unstable controller into the stable controller. The results of the stabilization of the coexisting unstable focus are shown in Fig. 14.

The robustness of the control algorithm enabled us to stabilize unstable steady states in the whole parameter region of interest. By mapping the stable and unstable phase objects, we managed to visualize bifurcations from experimental data. In Fig. 15, the stable steady states and limit cycles are

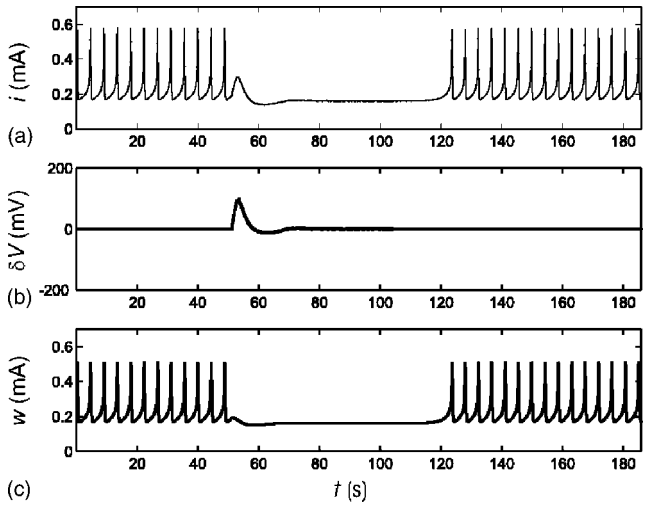

FIG. 13. The same as in Fig. 12 but for the control technique based on Eqs. (26) and (27), i.e., the current is used as a control signal. $k=800\ \Omega$, $\lambda^c=0.1\ s^{-1}$, $\delta V_{max}=200$ mV.

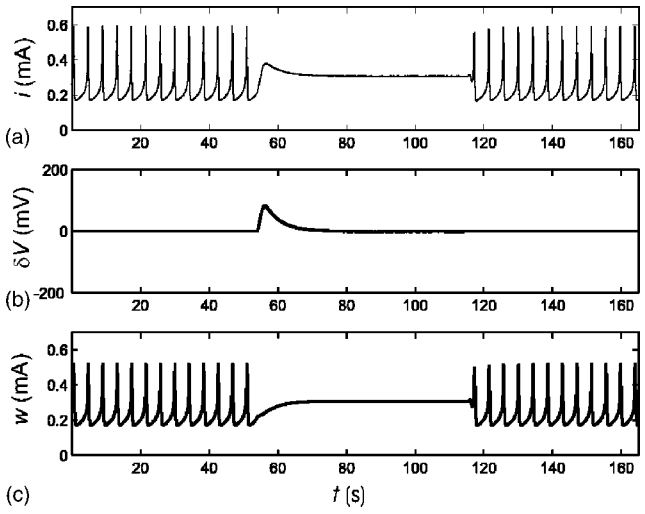

FIG. 14. Stabilization of the coexisting unstable focus by changing the sign of the parameter λ^c. All the parameters are the same as in Fig. 13, except λ^c, which here is equal to $-0.1\ s^{-1}$.

shown with the stabilized unstable states. At lower potentials [Fig. 15(a)], there is only a stable limit cycle and an unstable focus. As the potential is increased [Fig. 15(b)], new steady states (the saddle and the stable node) occur in the low-current region via a saddle node bifurcation. With further

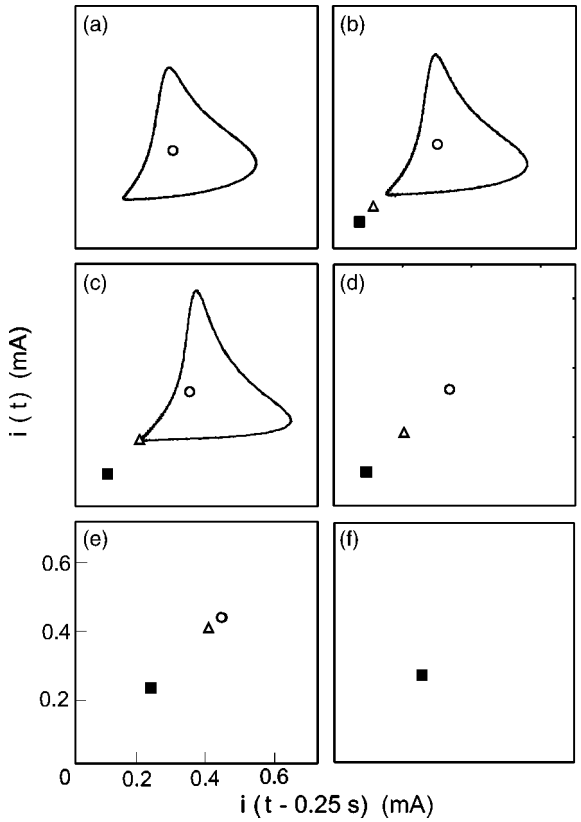

FIG. 15. Experimentally reconstructed phase portraits of different steady states (circle: high current unstable state, square: low-current stable state, triangle: saddle point) and the limit cycles (solid lines) at different circuit potentials V_0: (a) 1.200 V, (b) 1.220 V, (c) 1.260 V, (d) 1.270 V, (e) 1.380 V, (f) 1.410 V.

increase in the potential [Fig. 15(c)], the saddle point approaches the limit cycle; the limit cycle disappears with the collision of the saddle point [Fig. 15(d)], resulting in a saddle-loop (homoclinic) bifurcation. At larger potentials, the saddle approaches the upper steady state and disappears through another saddle node bifurcation. At large potentials [Fig. 3(f)], only one stable steady state exists. These phase portraits are in good qualitative agreement with the model results presented in Fig. 7. This implies that the control algorithm is a useful tool in experiments for reconstructing phase portraits of stable and unstable objects.

V. CONCLUSIONS

In this paper, we have considered a simple adaptive dynamic controller for stabilizing unknown unstable steady states of dynamical systems. It is similar to the delayed feedback controller, however the delay line is replaced with the low-pass filter. The controller is reference-free; it does not require knowledge of either the position of the fixed point in the phase space or the exact dynamical laws. The controller automatically finds and stabilizes the unstable fixed point in the phase space. Whenever the stabilization is attained, the feedback perturbation vanishes and there is no power dissipated in the feedback loop. The controller based on a conventional low-pass filter has a topological limitation similar to that of a delayed feedback controller; it cannot stabilize unstable steady states with an odd number of real positive eigenvalues. To overcome this limitation, we use an unstable low-pass filter that can stabilize saddle-type steady states of dynamical systems.

The efficiency of the adaptive controller is demonstrated for several models, namely a pendulum driven with a constant torque, the Lorenz system, and the electrochemical oscillator. The analysis of the basin of attraction of the stabilized fixed point shows that this basin can be essentially enlarged by a restriction of the feedback perturbation. With the method, both direct and indirect variables can be used for control; in the electrochemical example explored here, the use of the current, the indirect variable, was more efficient.

The experiments with the electrochemical nickel dissolution system confirm the robustness of the adaptive controller and demonstrate its capability of stabilizing unknown steady states in systems with unknown dynamical laws. Using this controller, we managed to reconstruct the phase portraits of the system directly from experimental data and detect various bifurcations that appear in the system when the control parameter is varied.

ACKNOWLEDGMENTS

This work was supported in part by the National Science Foundation (Grant No. CTS-0317762).

[1] R. Bellmann, *Introduction to the Mathematical Theory of Control Processes* (Academic Press, New York, 1971).
[2] H. Nijmeijer and A. Schaft, *Nonlinear Dynamical Control Systems* (Springer, New York, 1996).
[3] K. Ogata, *Modern Control Engineering* (Prentice-Hall, New York, 1997).
[4] G. Stephanopoulos, *Chemical Process Control: An Introduction to Theory and Practice* (Prentice-Hall, Englewood Cliffs, NJ, 1984).
[5] E. Ott, C. Grebogi, and J. A. Yorke, Phys. Rev. Lett. **64**, 1196 (1990).
[6] T. Shinbrot, C. Grebogy, E. Ott, and J. A. Yorke, Nature (London) **363**, 411 (1993).
[7] T. Shinbrot, Adv. Phys. **44**, 73 (1995).
[8] *Handbook of Chaos Control*, edited by H. G. Shuster (Wiley-VCH, Weinheim, 1999).
[9] S. Boccaletti, C. Grebogi, Y.-C. Lai, H. Mancini, and D. Maza, Phys. Rep. **329**, 103 (2000).
[10] K. Pyragas, Phys. Lett. A **170**, 421 (1992).
[11] H. Nakajima, Phys. Lett. A **232**, 207 (1997).
[12] K. Pyragas, Phys. Rev. Lett. **86**, 2265 (2001).
[13] S. Bielawski, M. Bouazaoui, D. Derozier, and P. Glorieux, Phys. Rev. A **47**, 3276 (1993).
[14] P. Parmananda, M. A. Rhode, G. A. Johnson, R. W. Rollins, H. D. Dewald, and A. J. Markworth, Phys. Rev. E **49**, 5007 (1994).
[15] K. Pyragas, Phys. Lett. A **206**, 323 (1995).
[16] A. Namajūnas, K. Pyragas, and A. Tamaševičius, Phys. Lett. A **204**, 255 (1995).
[17] N. F. Rulkov, L. S. Tsimring, and H. D. I. Abarbanel, Phys. Rev. E **50**, 314 (1994).
[18] M. Ciofini, A. Labate, R. Meucci, and M. Galanti, Phys. Rev. E **60**, 398 (1999).
[19] A. Schenck zu Schweinsberg and U. Dressler, Phys. Rev. E **63**, 056210 (2001).
[20] R. Meucci, R. McAllister, and R. Roy, Phys. Rev. E **66**, 026216 (2002).
[21] K. Pyragas, V. Pyragas, I. Z. Kiss, and J. L. Hudson, Phys. Rev. Lett. **89**, 244103 (2002).
[22] K. Ogata, *Modern Control Engineering* (Prentice Hall, Englewood Cliffs, NJ, 1990).
[23] E. N. Lorenz, J. Atmos. Sci. **20**, 130 (1963).
[24] M. Gorman, P. J. Widmann, and K. A. Robbins, Phys. Rev. Lett. **52**, 2241 (1984).
[25] M. Gorman, P. J. Widmann, and K. A. Robbins, Physica D **19**, 255 (1986).
[26] D. Haim, O. Lev, L. M. Pismen, and M. Sheintuch, J. Phys. Chem. **96**, 2676 (1992).